Microchimica Acta (2022) 189:409
https://doi.org/10.1007/s00604-022-05498-w

ORIGINAL PAPER

# Electrocatalytic oxidation and amperometric determination of sulfasalazine using bimetal oxide nanoparticles–decorated graphene oxide composite modified glassy carbon electrode at neutral pH

**Umamaheswari Rajaji[1] · Raghu M.S.[2] · Yogesh Kumar K.[3,4] · Abdullah A. Al-Kahtani[5] · Chih-Ping Chen[1] · Ruey-Shin Juang[6,7,8] · Ting-Yu Liu[1,9,10]**

Received: 5 April 2022 / Accepted: 13 September 2022 / Published online: 7 October 2022


## Abstract

Cube-shaped samarium orthovanadate ($SmVO_4$) nanoparticles were interconnected with a graphene oxide sheet (GOS) using a simple and eco-friendly method to generate a $SmVO_4$@GOS nanocomposite. $SmVO_4$ was characterized using various spectroscopic and microscopic techniques, which confirmed the wrapping of GOS around the $SmVO_4$ nanoparticles. $SmVO_4$@GOS was then used to modify a glassy carbon electrode (GCE), which was evaluated for its electrochemical performance toward the assay of sulfasalazine (SSZ), an antibiotic drug. Cyclic voltammetry and amperometry were both used for the assay of SSZ using the $SmVO_4$@GOS-modified GCE at pH 7. The modified amperometric sensor is more sensitive, with a low detection limit (2.16 nM) and wide linear range of 20 nM–667 µM (Ag/AgCl). The electrochemical oxidation of SSZ was tested with blood serum and urine samples at physiological pH with recoveries in the range 96.1–98.6%. It indicates that the modified electrochemical sensor has good sensitivity and practical applicability toward SSZ detection. In the field of non-enzymatic sensors, $SmVO_4$@GOS/GCE provides a highly promising performance. Therefore, the electrochemical sensors have capacity for extensive analytical applications in biomedical devices.

**Keywords** Electrochemical detection · Cyclic voltammetry · Amperometry · Graphene oxide sheets · Transition metal oxides · Drug determination · Biological analysis

✉ Chih-Ping Chen
cpchen@mail.mcut.edu.tw

✉ Ruey-Shin Juang
rsjuang@mail.cgu.edu.tw

✉ Ting-Yu Liu
tyliu0322@gmail.com

Umamaheswari Rajaji
umachemist24@gmail.com

[1] Department of Materials Engineering, Ming Chi University of Technology, New Taipei City 243303, Taiwan

[2] Department of Chemistry, New Horizon College of Engineering, Outer Ring Road, Bangalore 560103, India

[3] Department of Chemistry, Faculty of Engineering and Technology, Jain University, Bangalore 562112, India

[4] Korea University of Technology and Education, Cheonan-si 31253, Chungcheongnam-do, Cheonan-si, Republic of Korea

[5] Chemistry Department, College of Science, King Saud University, P.O. Box 2455, Riyadh 11451, Saudi Arabia

[6] Department of Chemical and Materials Engineering, Chang Gung University, 259 Wenhua First Road Guishan, Taoyuan 33302, Taiwan

[7] Division of Nephrology, Department of Internal Medicine, Chang Gung Memorial Hospital, Linkou, Taiwan

[8] Department of Safety, Health and Environmental Engineering, Ming Chi University of Technology, Taishan, New Taipei City 243303, Taiwan

[9] Research Center for Intelligent Medical Devices, Center for Plasma and Thin Film Technologies, Ming Chi University of Technology, New Taipei City 243303, Taiwan

[10] Department of Chemical Engineering and Materials Science, Yuan Ze University, Taoyuan City 32003, Taiwan

## Introduction

Sulfasalazine (SSZ) is a sulfonamide-type drug and is sold under the trade names Azulfidine, Salazopyrin, and Sulazine. SSZ is an antibiotic class of drug used extensively for the treatment of various inflammatory bowel diseases such as ulcerative colitis and Crohn's disease [1–4]. In addition, SSZ is used to treat rheumatoid arthritis, which is associated with psoriatic and reactive arthritis [5]. SSZ consists of an azo bond, which connects the sulfonamide of pyridyl benzene with salicylic acid. Adverse effects from the continuous intake of SSZ occur in 3–20% of patients, which can lead to cancer and hemopoietic disorders. Physicians therefore need to be aware of the dosage given and the amount of SSZ present in the serum. According to medical researchers, the acceptable SSZ content in serum during treatment is 6–32 $\mu g \cdot mL^{-1}$ [1]. In addition to the dose, oral consumption of SSZ may lead to health risks such as obstruction in the urinary tract and intestines and the severe accumulation of kidney stones. To avoid risks associated with overdosing, easy and fast detection of SSZ in serum can minimize adverse effects on patients. Recently, sulfasalazine residue has been found in the ecosystem owing to improper disposal, and 25% of sulfa drugs can cause folate deficiency, kidney stones, megaloblastic anemia, and hemolytic anemia [5, 6]. There are several reports in the literature regarding the assay of SSZ using UV–visible spectrophotometry, high-performance liquid chromatography (HPLC), solid-phase extraction coupled with capillary electrophoresis, and gas chromatographic–tandem mass spectroscopic techniques (GC–MS) [6–10]. However, these methods have issues related to sensitivity, selectivity, range of detection, and interference in real-world samples; they are also tedious and require expertise. The electrochemical sensors are an alternative to overcome the above limitations, providing sensitive, precise, and accurate results with a low limit of detection (LOD) toward the SSZ assay. Tremendous effort has been made by researchers across the globe to fabricate materials for the surface modification of electrochemical sensor electrodes; these materials include carbon-based nanomaterials (i.e., carbon nanotubes, graphene, and graphene oxide), nanoparticles and nanocomposites, polymeric materials, and ionic liquids [11, 12]. Materials used for electrochemical sensors should possess good conductivity, speed up electron transfer kinetics, and have the capacity to oxidize a given drug molecule. At present, rare-earth metals/metal vanadates are generating much interest among researchers in terms of their electrochemical performance in supercapacitors, solar cells, batteries, sensors, and so on. Rare-earth metals exhibit a 4f structure, which enhances electrochemical behavior and provides several paths for electron transition.

Recently, rare-earth metal vanadates have been receiving increased attention from material scientists as they possess high stability, low toxicity, multiple valence states, rich oxygen vacancies, good energy density and conductivity, and tunable band gaps [9, 13–15]. Transition metal–based vanadates have been used in various fields such as energy storage, gas sensors, solar cells, electrochemical sensors, and supercapacitors because they possess admirable energy gaps and stable structures. $CeVO_4$, $PrVO_4$, $LuVO_4$, and $SmVO_4$ nanoparticles have been exploited as electrode materials for the detection of drug molecules [16–18]. Among these, Sm-based vanadates are important because of their mixed oxidation states (+2 and +3), higher ionic conductivity, elevated ionic radius (1.08 Å), great surface basicity, and low critical voltage. Usually, $SmVO_4$ exhibits two crystalline phases, namely, monoclinic (monazite m-type) and tetragonal (t-type) [19]. Lanthanides in general show better coordination with the m-type crystalline phase than with the t-type phase owing to their high coordination number [20–23]. Hence, $SmVO_4$ in a monoclinic phase is thermally more stable than that in a metastable tetragonal phase. Synthesis of tetragonal-phase $SmVO_4$ using conventional methods is very complicated, and it is challenging to synthesize $SmVO_4$ without using toxic solvents and surfactants. The few reports on the synthesis of $SmVO_4$ in the literature mainly focus on photocatalytic studies of $SmVO_4$ [24, 25]. Reports on the electrochemical detection of SSZ mention the use of a glassy carbon electrode (GCE), poly(3-methylthiophene) coated on GCE, GO/$Fe_3O_4$@$SiO_2$/CPE, NiO NPs-CPE, NiO/CNT CPE, and MWCNTCOOH/BA-SPCE as electrode modifiers and electrodes. However, these materials lack sensitivity and selectivity in the electrochemical detection of SSZ. To date, there has been no report on the electrocatalytic performance of $SmVO_4$ for the detection of anti-rheumatic drugs. Still, $SmVO_4$ in its pure tetragonal phase is not beneficial for electrochemical sensors because such a structure reduces the conductivity, which in turn increases the resistivity owing to the blockage of electron–hole pairs [26, 27].

These limitations of $SmVO_4$ could be overcome by doping with metal oxides, metallic and non-metallic ions, organic semiconductors, additives, carbon-based materials, and so on [28]. Among these, carbon-based materials such as carbon nanotubes (CNTs), graphene oxide sheets (GOSs), carbon spheres, and g-$C_3N_4$ are better supporting materials for metal orthovanadates. GOSs are beneficial owing to their enhanced surface area, increased mechanical strength, flexibility, and good conductivity [29–32]. Because of the superior performance of graphene in biochemical sensors as a result of its large specific surface area, ease of modification, wide potential window, high electron transfer rate, high charge-carrier mobility, and low electrical noise levels [33, 34], it can be used for highly sensitive detection, efficient receptor immobilization, easy

interaction with biomolecules, and promotion of electron transfer between reagents and graphene [35–39]. Graphene oxide is easily dispersed in organic solvents, water, and other matrices because of the presence of oxygen functions. This is a significant advantage when graphene oxide is combined with polymers or ceramic matrixes to improve its mechanical and electrical characteristics. Graphene-based biochemical sensors outperform traditional carbon electrode–based sensors in terms of sensitivity, LOD, and reaction time. As a result, a variety of graphene-based biochemical sensors for health monitoring have been presented (Scheme 1). The abovementioned properties of two-dimensional (2D) graphene sheets are additional advantages in the electrochemical detection of drugs in pharmaceutical research. For any electrochemical application, the sheet-like structure of the material facilitates electron mobility and electrolyte diffusion.

In the present study, we synthesized single-crystalline $SmVO_4$ nanoparticles wrapped with GOSs ($SmVO_4$@GOS) using a deep eutectic solvent via the hydrothermal method. The as-prepared $SmVO_4$@GOS electrocatalyst was used to modify a GCE, and we evaluated the electrochemical performance of the modified GCE using cyclic voltammetry (CV), electrochemical impedance spectroscopy (EIS), and amperometric analysis (AMP). The modified GCE exhibited better electrochemical characteristics for SSZ detection compared to a bare GCE. The selectivity of the $SmVO_4$@GOS/GCE was further evaluated by detecting SSZ in blood serum and human urine samples. The obtained electrochemical and actual sample results, recovery percentage, concentration range, and LOD values indicated that $SmVO_4$@GOS/GCE could serve as an alternate material for the simple, swift, and sensitive detection of SSZ in active pharmaceutical ingredients and formulations and in real-world samples.

## Experimental section

### Materials and methods

Samarium(III) nitrate hexahydrate ($Sm(NO_3)_3{\cdot}6H_2O$; 99.9%), ammonium metavanadate ($NH_4VO_3$; ACS reagent, ≥ 99.0%), urea (ACS reagent, 99.0–100.5%), polyethylene glycol (PEG; average molecular weight—6000), sulfasalazine (analytical grade, 98.0–101.5%), and all other chemicals were procured from Sigma-Aldrich (https://www.sigmaaldrich.com/TW/en) and used without further purification. Phosphate buffer (PB, 0.05 M) was prepared using $NaH_2PO_4$ (≥ 99.0%) and $Na_2HPO_4$ (≥ 99.0%), and diluted HCl/NaOH was used to prepare buffers with different pH values. Graphene oxide was synthesized using the modified Hummers method. The methods and experimental details for these materials are given in the Supporting information. Human blood serum and urine samples were collected from the Chang Gung Memorial Hospital, Taiwan.

TEM images were obtained using a JEOL JEM-2100F instrument operating at 200 kV. SEM was obtained using HAADF-SEM, and the energy-dispersive X-ray analysis (EDS) device fitted with an electron microscope was used to examine the elemental composition of a sample. Elemental analysis was ascertained using an elemental

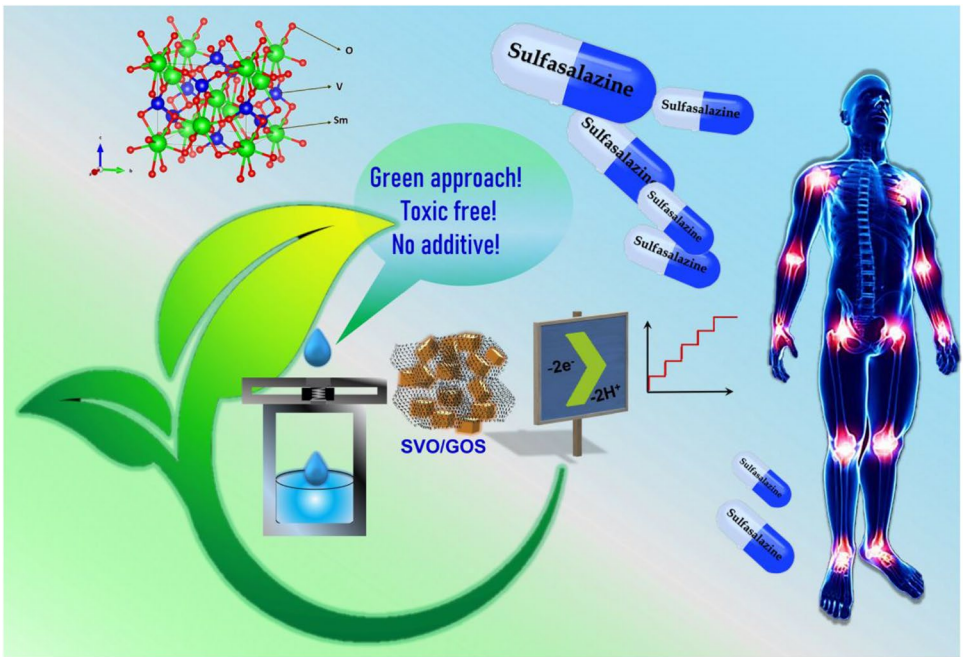


**Scheme 1** Synthesis of metal vanadate–related bimetal oxide nanoparticles with a graphene oxide composite for electrochemical applications

analyzer (Perkin Elmer, Series II 2400). XPS measurements were conducted on a PHI 5000 Versa probe II scanning XPS microprobe (ULVAC-PHI) spectrometer equipped with Al-Kα X-ray radiation ($h\nu = 1486.6$ eV). Wide-angle X-ray diffraction patterns were recorded on a PANalytical X'Pert PRO diffractometer using graphite-monochromatic Cu-Kα radiation ($\lambda = 0.1541$ nm), and samples were scanned from 5 to 75° at a rate of 5° $min^{-1}$. High-performance liquid chromatography (HPLC) was used on a Waters Alliance e2695 (250 × 4.6 mm) with an ALPHA 10 isocratic pump; fractions were detected with a TOPAZ dual UV detector, and data was analyzed using the Peak-ABC software. Methanol and acetic acid (mobile phase) were used (flow rate = 0.6 mL/min, $\lambda = 300$ nm). CV experiments were carried out on a CHI 1205A analyzer electrochemical workstation (USA working station). A conventional three-electrode system consists of an Ag/AgCl (saturated KCl) electrode as the reference electrode, a platinum wire as the auxiliary electrode, and $SmVO_4$/GOS modified GCE (glassy carbon electrode) as the working electrode.

### *Green synthesis of $SmVO_4$ NPs and $SmVO_4$@GOS*

Samarium orthovanadate nanocubes were synthesized by the hydrothermal method. $NH_4VO_3$ (10 mmol) and 5 mmol $Sm(NO_3)_3{\cdot}6H_2O$ were dissolved in a 2:1 (PEG–urea) deep eutectic solvent. The nanocubes were transferred to a Teflon-coated hydrothermal autoclave and placed in an oven at 180 °C for 12 h. The obtained precipitate was washed with distilled water and ethanol several times and dried in an oven overnight. The resultant powder comprised $SmVO_4$ nanoparticles. The GOS (5 mg) [40] and 5 mg of $SmVO_4$ were dissolved in deionized (DI) water and ultrasonicated for 30 min. The resulting compound was denoted as $SmVO_4$@GOS. A schematic representation of the synthesis procedure is given in Scheme 2. Details on the materials and methods used for the synthesis of GOS are given in the Supporting information file.

### *Fabrication of $SmVO_4$@GOS modified GCE*

A GCE working electrode was modified using $SmVO_4$@GOS. First, the GCE was polished using 0.05-µm alumina powder and sonicated in water. The suspension (2 mg $mL^{-1}$) was dispersed in DI water through sonication, and 7 µL of the suspension was drop casted on GCE and used after drying at 65 °C.

## Results and discussion

### Choice of materials

Various bimetal oxides and vanadate materials such as $MnCo_2O_4$, $CoVO_4$, ZnO–$Co_3O_4$, GO/$Fe_3O_4$, and $SmVO_4$ nanoparticles have been used to develop selective and sensitive drug detection sensors. Among them, $SmVO_4$ particles have gained wide acceptance for the trace determination of SSZ when used with a composite modified GCE owing to their high electrical conductivity, the ability to form composites with many carbon materials, simple preparation, wide potential window, and insensitivity to dissolved oxygen. More importantly, $SmVO_4$ showed good electrochemical response to SSZ in previous experiments.

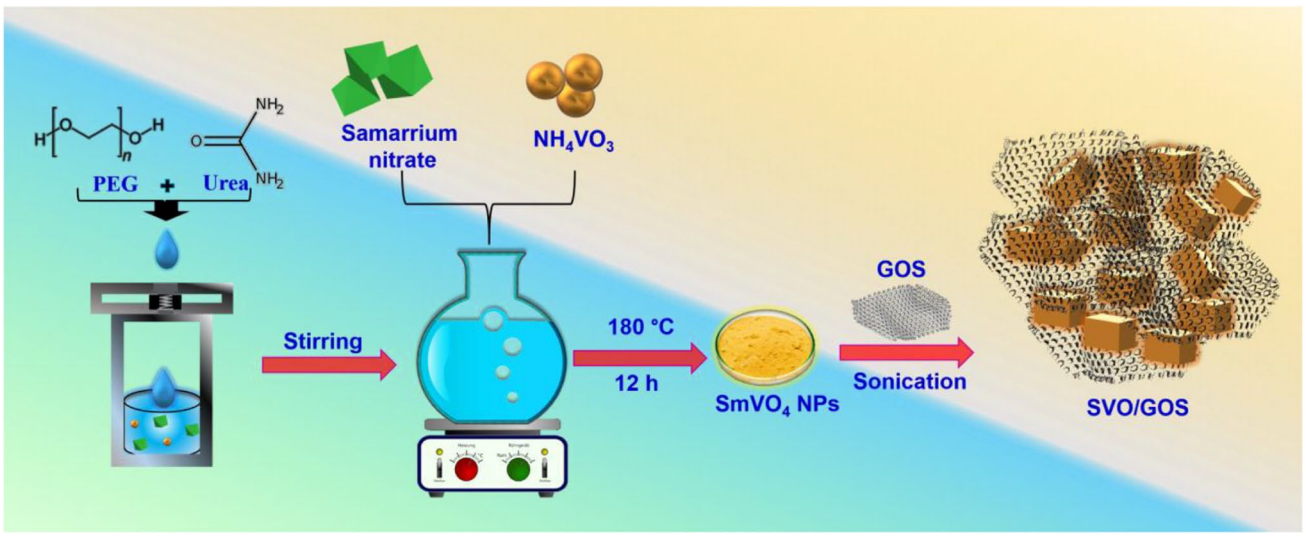


**Scheme 2** Schematic of the synthesis of the $SmVO_4$@GOS composite and electrocatalytic application

Nanomaterials have been widely used to construct electrochemical sensors because of their various shapes, sizes, and compositions, which can increase the analytical selectivity and sensitivity. In particular, GOS-related materials have been a hot research topic in the past few years because of their unique construction. The many functional groups on the surface of GOSs can interact with samarium vanadates, which facilitates the formation of the composite. The excellent absorption property and large surface area of the unique GOS structure combined with the abilities of $SmVO_4$ provided a potential electrode material for the detection of SSZ.

### *Chemical composition of the $SmVO_4$@GOS composite*

The crystalline structure and phase of nanocomposites are important features in determining their electrochemical characteristics. The X-ray diffraction (XRD) patterns of the synthesized GOSs and $SmVO_4$@GOS are given in Fig. 1A. The characteristic peaks of $SmVO_4$ at (101), (200), (211), (112), (220), (301), (103), (321), (312), (400), (411), (420), (332), (204), (431), and (224) are well correlated with standard JCPDS no. 87–1526 and indicate the metastable tetragonal phase [41]. A slight broad hump observed at $2\theta = 10.7°$ with (001) indicates (JCPDS card no. 41–1487) the effective wrapping of GOS around the $SmVO_4$ nanoparticles [42]. The crystalline size of $SmVO_4$@GOS was calculated using Eq. (1).

$$D_P = (k\lambda/\beta cos\theta) \quad (1)$$

where $D_P$ is the grain size of the particle (nm), $k$ is the Scherrer constant ($k = 0.94$), $\lambda$ is the X-ray wavelength (1.54178 Å), $\beta$ is the full width at half maximum (FWHM) of the diffraction peak, and $\theta$ is the angle of diffraction. The calculated average size of $SmVO_4$@GOS was found to be 124.7 nm for the major peaks.

To better understand the elemental interactions of $SmVO_4$@GOS, XPS analyses were conducted and the obtained survey spectra of GOS and $SmVO_4$@GOS are given in Fig. 1B. Figure 2A represents the high-resolution X-ray photoelectron spectroscopy (XPS) spectrum of Sm, which exhibits two characteristic peaks at 1085 and 1112 eV, attributed to $Sm^{3+}$ $3d_{3/2}$ and $3d_{5/2}$, respectively. The XPS spectrum of V is depicted in Fig. 2B. It consists of $V2p_{1/2}$ and $2p_{3/2}$ peaks at 528.35 eV and 521.44 eV, respectively, indicating the + 5 oxidation state of V [43, 44]. Peaks between 535 and 529 eV are observed in Fig. 2C indicating the presence of O 1 s [45, 46]. Peaks at 280 to 298 eV (Fig. 2D) belong to C 1 s and disclose the presence of C–C, C–O, and C = O of GOS [45]. These XPS results clearly indicate the formation of a $SmVO_4$@GOS composite.

### *Morphological analysis of the $SmVO_4$@GOS composite*

The morphology and shape of the as-prepared $SmVO_4$@GOS composite were evaluated by using field emission scanning electron microscopy (FESEM) and transmission electron microscopy (TEM). Figure 3 A1–A3 show the FESEM images of the composites. The $SmVO_4$ particles clearly have a cube-shaped structure less than 100 nm across and approximately 30–70 nm thick. There are also some small

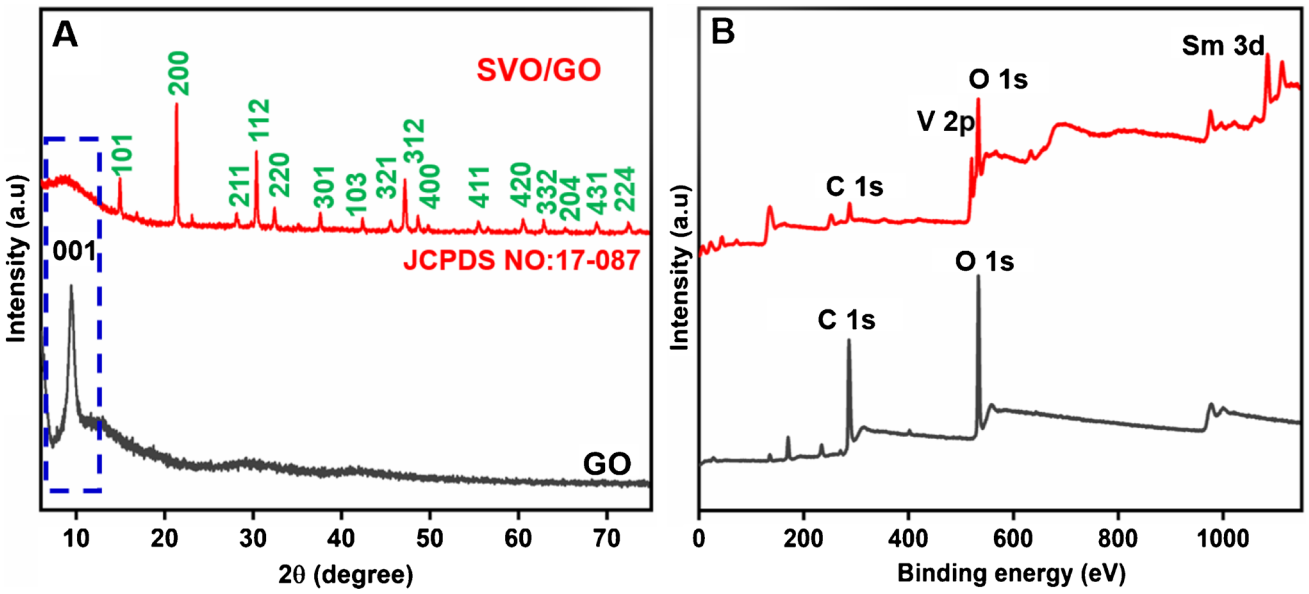


**Fig. 1** **A** XRD patterns of GOS and $SmVO_4$@GOS. **B** XPS analyses of GOS and $SmVO_4$@GOS

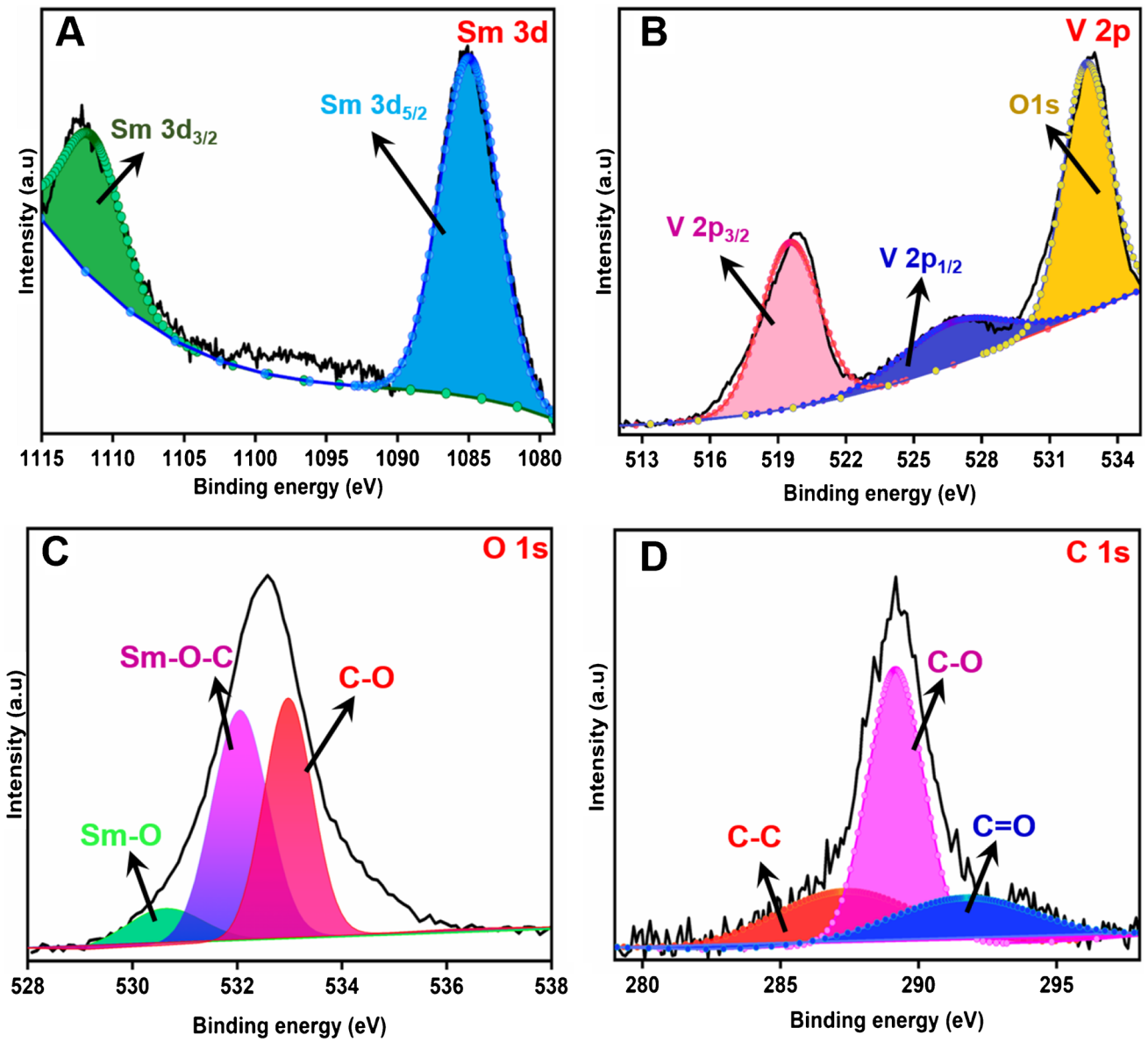


**Fig. 2** XPS analyses of **A** Sm 3d, **B** V 2p, **C** O 1 s, and **D** C1s

irregular particles attached to the surface. Closer observation of the $SmVO_4$@GOS nanocomposite clearly indicates the layer-by-layer stacking of GOS wrapped around the $SmVO_4$ nanoparticles. It was not possible to distinguish between the $SmVO_4$ and GOS phases in the FESEM images, possibly because of the poor phase contrast. Therefore, the materials were further subjected to TEM studies (Fig. 3B1–B3), which confirmed the wrapping of the GOS layer around the nanoparticle surface. It was clearly indicated that thin layers of GOS and cube-shaped SmVO4 particles were interconnected with each other in Fig. 3B3. The figure also shows the clear contact between the $SmVO_4$ nanoparticles and the GOSs, which is essential for improving the electron transfer reaction. The TEM images also revealed that this wrapped material was evenly dispersed, which may facilitate the quick access of ions and electrons to the active surfaces, thereby allowing a quick transfer reaction. This would result in better output and thus better power performance. Energy-dispersive X-ray spectroscopy (EDS) analysis and mapping were carried out for the as-synthesized materials. Figure 3C-F display the mapping images of $SmVO_4$@GOS, in which Sm, V, O, and C are uniformly distributed. Figure 3G shows the EDS profile of $SmVO_4$@GOS, which confirms the elements of Sm, V, O, and C.

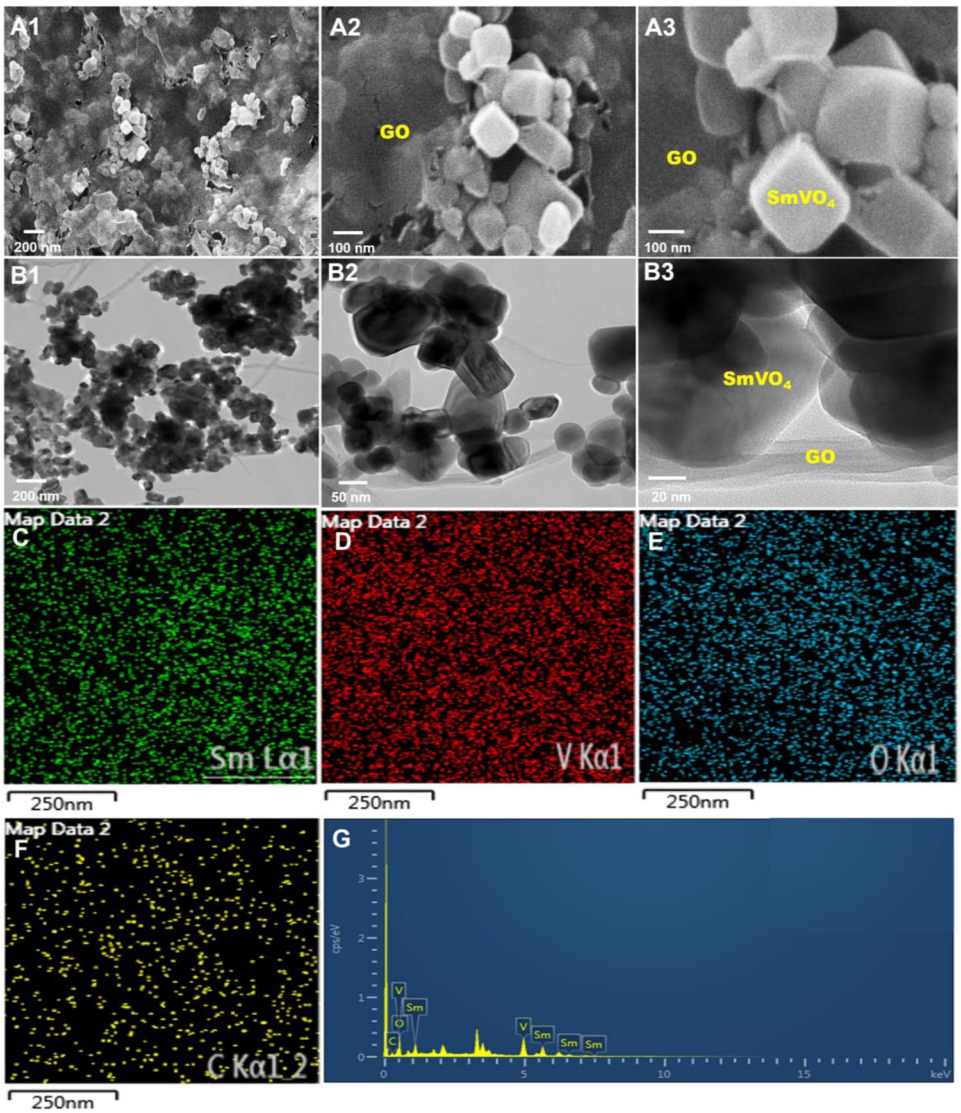


**Fig. 3** **A1**–**A3** SEM and **B1**–**B3** TEM images of $SmVO_4$@GOS. **C**–**F** Elemental mapping images and **G** elemental analysis of $SmVO_4$@GOS

### *Electrochemical characterization of the $SmVO_4$@GOS electrode*

The electrical resistance and interface between the electrolyte and the surface of an electrode are key features of an electrochemical sensor, which was investigated using EIS. The obtained Nyquist plots of bare GCE, GOS/GCE, $SmVO_4$/GCE, and $SmVO_4$@GOS/GCE in 0.1 M KCl in the presence of 5 mM $[Fe(CN)_6]^{-3/-4}$ are given in Fig. 4A. The semicircular portion of $SmVO_4$@GOS/GCE is relatively small compared to those of GCE and GOS/GCE. The $R_{ct}$ values (Fig. 4A, inset) for the three different electrodes were computed and found to be 52.63 Ω, 61.02 Ω, 118.26 Ω, and 234.12 Ω for $SmVO_4$@GOS/GCE, $SmVO_4$/GCE, GOS/GCE, and bare GCE, respectively. The lowered resistance of the $SmVO_4$@GOS nanocomposite was owing to the increased conductance and larger surface area, which facilitated the diffusion and mobility of electrons in the electrolyte medium [47, 48]. The electrochemical active surface area was calculated by the CV method, and the surface area of $SmVO_4$@GOS/GCE was found 0.141 $cm^2$ using the Randles–Sevcik equation.

## Optimization of the electrochemical conditions and electrodes

The quantity of the composite used on the surface of an electrode plays a vital role in the electrochemical performance of the electrode. The concentration of $SmVO_4$@GOS was varied from 0.5 to 2.5 mg $mL^{-1}$ in 0.05 M phosphate buffer (PB; pH 7.0) at a 0.05 V $s^{-1}$ scan rate. The obtained plot is given in Fig. S1A. The figure indicates that the anodic current response increased continuously toward the oxidation of SSZ as the concentration of $SmVO_4$@GOS increased from 0.5 to 2.5 mg $mL^{-1}$. With a further increase in the

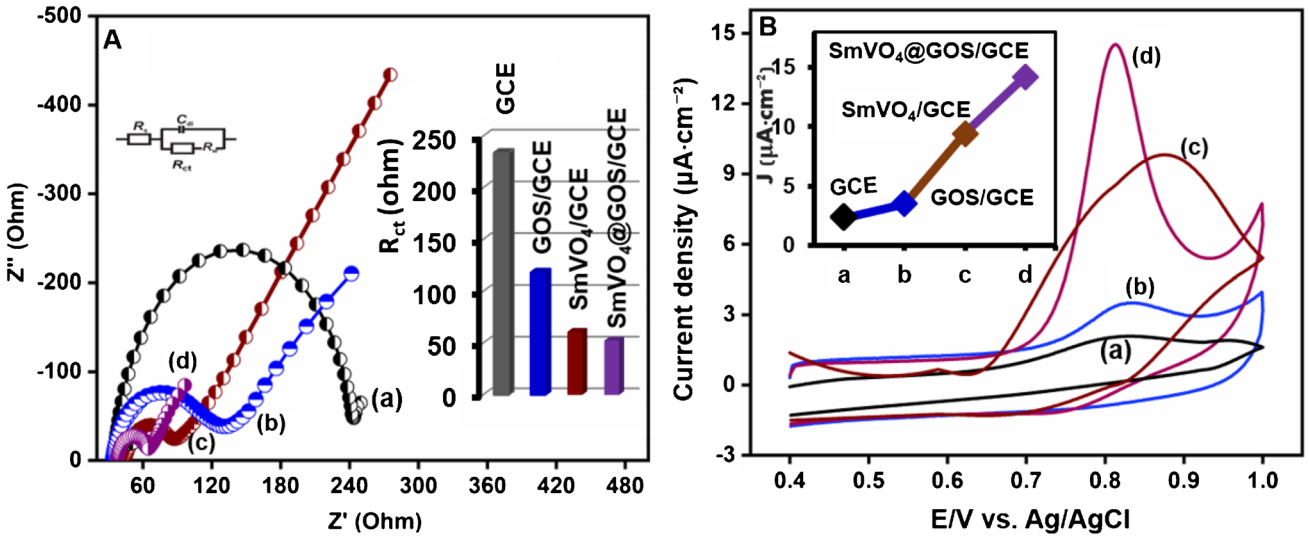


**Fig. 4** **A** EIS patterns of (a) bare GCE, (b) GOS/GCE, (c) $SmVO_4$/GCE, and (d) $SmVO_4$@GOS/GCE in 5 mM $[Fe(CN)_6)]^{3-/4-}$ containing 0.1 M KCl as the electrolyte (inset: Randles circuit). **B** CV responses for 100 μM SSZ at (a) bare GCE, (b) GOS/GCE, (c) $SmVO_4$/GCE, and (d) $SmVO_4$@GOS/GCE in 0.05 M PB (pH = 7) at a 50 mV $s^{-1}$ scan rate

concentration (1.0 mg $mL^{-1}$), the current response toward the oxidation of SSZ decreased because of the blocking of active sites at high concentrations of the nanocomposite. The highest oxidation peak current was achieved for 1.0 mg $mL^{-1}$, which was thus the optimal concentration of $SmVO_4$@GOS for the detection of SSZ. Furthermore, coating of $SmVO_4$@GOS volume was optimized. Seven microliters of the composite modified electrode has achieved high peak current. The data are given in Fig. S1B of the Supporting information.

### *Electrocatalytic activity of $SmVO_4$@GOS/GCE in phosphate buffer*

SSZ oxidation using different materials on the electrode was carried out. The CV responses of 100 μM of SSZ in 0.05 M PB (pH 7) at a scan rate of 0.05 V $s^{-1}$ in the presence of bare GCE, GOS/GCE, $SmVO_4$/GCE, and $SmVO_4$@GOS/GCE are shown in Fig. 4B. The low conductivity between GCE and the electrolyte resulted in poor electrochemical performance. The GOS/GCE exhibits a small hump, indicating a slight anodic current response of 3.4 μA compared to the bare GCE at the same potential. The maximum anodic peak current is observed for the $SmVO_4$@GOS/GCE at a similar potential, with a high current response of 14.2 μA. This confirms the excellent capacity of $SmVO_4$@GOS/GCE toward the detection of SSZ in 0.05 M PB owing to the enhanced conductivity of the modified GCE.

Figure 5A shows the impact of SSZ concentration in the range of 25 to 275 μM at a 0.05 V $s^{-1}$ scan rate in 0.05 M PB (pH 7). The results indicate that the anodic peak current response increased with increasing SSZ concentration owing to its effective oxidation. The linearity plot of SSZ concentration against current is given in the inset in Fig. 5A, which shows good linearity with the regression equation $y = 0.431$ [μM] + 0.21 and $R^2 = 0.9897$. This regression equation indicates that the oxidation of SSZ at $SmVO_4$@GOS/GCE follows that of antifouling reactions. To study the effect of the scan rate on the oxidation of SSZ, the scan rate was varied from 0.02 to 0.2 V $s^{-1}$, and the obtained response is shown in Fig. 5B. The figure shows an increase in anodic peak current with an increasing scan rate, with a slight shift in the anodic peak toward higher potentials. The inset in Fig. 5B shows the calibration plot of anodic current against the square root of the scan rate, where the regression equation $y = 5.313x + 0.4201$ and $R^2 = 0.985$ clearly indicate the diffusion control process involved in the electrochemical oxidation of SSZ in 0.05 M PB in the presence of $SmVO_4$@GOS/GCE (Scheme 3).

The medium in which the electrochemical reaction occurs is also important in electrochemical sensors. Hence, the CV response was recorded for the oxidation of SSZ using $SmVO_4$@GOS/GCE at different pH values. The evaluation was performed for 50 μM SSZ at a 50 mV $s^{-1}$ scan rate, and the pH was varied from 6 to 10 (Fig. S2). Figure 6 indicates the drastic change in the CV response with respect to its shape, with irreversible peaks for the oxidation of SSZ. At lower pH values, a lower peak current is observed, and the maximum peak occurs at pH 7. Upon increasing the pH to alkaline (8–10), a gradual decrease in the anodic peak current is observed. This indicates that 0.05 M PB at pH 7 is the optimal pH value for the effective oxidation of SSZ using $SmVO_4$@GOS/GCE.

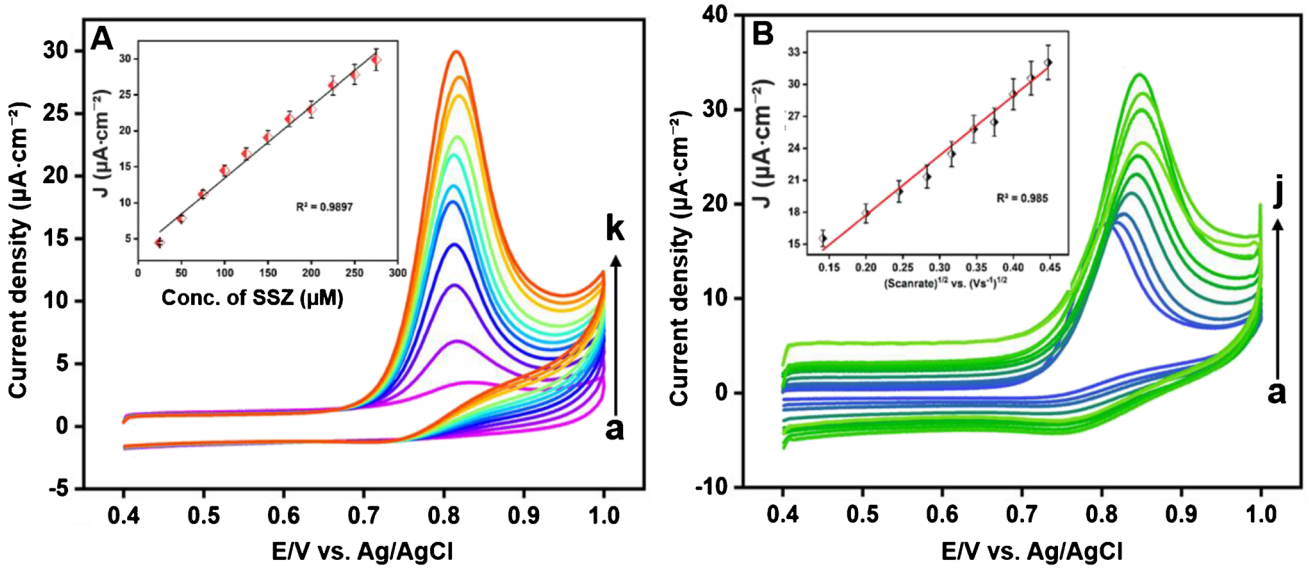


**Fig. 5** **A** CV of $SmVO_4$@GOS/GCE for different quantities of SSZ (25 to 275 μM) in 0.05 M PB (pH = 7). Inset: corresponding linear dependence plot between the concentration of SSZ (μM) and current density (μA·cm$^{-2}$). **B** CV curves of $SmVO_4$@GOS/GCE containing 100 μM SSZ at scan rates of 0.02–0.2 V s$^{-1}$ in 0.05 M PB (pH = 7). Inset: corresponding linear calibration plot for the square root of the scan rate (V s$^{-1}$) vs. current density (μA·cm.$^{-2}$)

The corresponding calibration plot of $E_{pa}$ versus pH is represented in Fig. S3. Moreover, the regression equation is noted as $E_{pa} = -0.053\ pH + 1.13$ ($R^2 = 0.991$). A slope value of 53 mV pH$^{-1}$ is close to the theoretical Nernstian value, specifying an equivalent number of electrons and proton movement in the electrochemical reaction. This maximum response at neutral pH is advantageous as most studies in the biological and medical fields take place at this pH. At neutral pH, the drug under study, SSZ, underwent an irreversible electro-oxidation process according to the 2e$^-$ and 2H$^+$ transfer mechanism given in Scheme 3 [1, 2].

The electrochemical performance of $SmVO_4$@GOS/GCE toward the oxidation of SSZ was also investigated through AMP studies at 0.82 V (Ag/AgCl). The AMP response was evaluated to understand the range, LOD, and sensitivity. Figure 6A , B depict the amperometric profile of SSZ detection using $SmVO_4$@GOS/GCE in 0.05 M PB (pH = 7) at a 0.05 V s$^{-1}$ scan rate. The oxidation peak current increases steadily with the

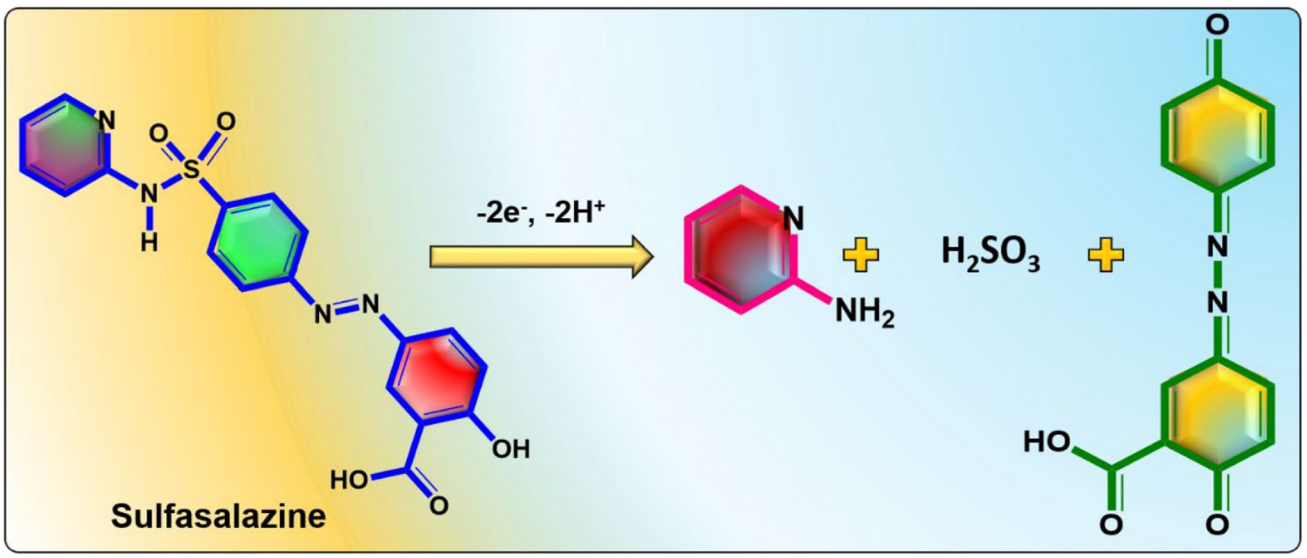


**Scheme 3** Electro-oxidation of SSZ at $SmVO_4$@GOS/GCE in 0.05 M PB (pH 7)

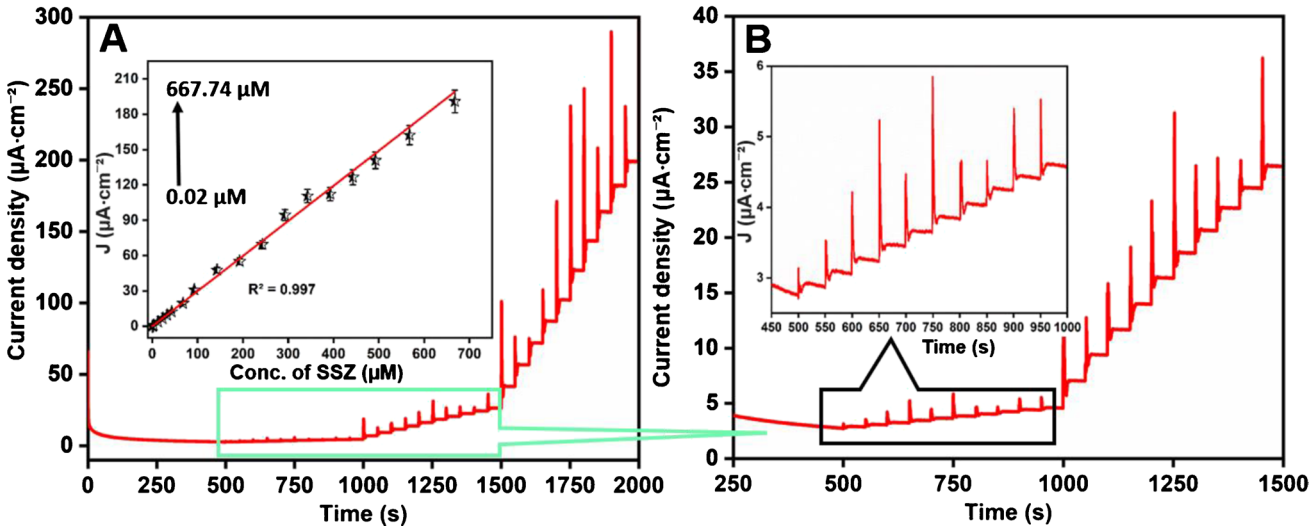


**Fig. 6** **A**, **B** Amperometric responses of $SmVO_4$@GOS/GCE for different quantities of SSZ (0.02–667 µM) in 0.05 M PB with pH = 7 at 0.82 V (rotation speed, 1200 rpm). Inset: corresponding linear dependence plot for the concentration of SSZ (µM) vs. current density (µA·cm.$^{-2}$)

sequential addition of SSZ. The calibration plot of current against concentration of SSZ (Fig. 6A, inset) shows a linear relationship, having a linear regression equation of $I_{pa}$ (µA) = 1.246 [µM] + 0.813 and a coefficient of $R^2 = 0.997$. The amperometric response toward the oxidation of SSZ covered a wide range of detection, from 0.02 to 667 µM, with 6.23 µA µM$^{-1}$ cm$^{-2}$ sensitivity and a 2.16 nM LOD value. The achieved sensitivity and LOD value for the detection of SSZ using $SmVO_4$@GOS/GCE are superior to those of many earlier reported methods, as given in Table 1, and thus should be of great interest.

Because many pharmaceutical formulations consist of one or more combinations of active drugs, selectivity toward the detection of individual components is a significant characteristic of an $SmVO_4$@GOS/GCE electrochemical sensor. The selectivity analysis was performed with a 20-fold higher concentration of SSZ, along with the following possible interfering analytes: uric acid

**Table 1** Analytical parameters for determining sulfasalazine at $SmVO_4$@GOS/GCE

| Modified electrode | Linear range (µM) | Sensitivity (µA µM$^{-1}$ cm$^{-2}$) | LOD (µM) | Method | Ref |
|---|---|---|---|---|---|
| Antimony film–modified GCE | 3–250 | – | 0.78 | SWV | [49] |
| GCE | 10–50 | – | 3.43 | DPV | [50] |
| Poly (3-methylthiophene)-coated GCE | 0.75–320 | 0.257 | 0.25 | SWV | [51] |
| GO/$Fe_3O_4$@$SiO_2$/CPE | 1–300 | – | 0.4 | LSV | [2] |
| NiO NP-CPE | 0.009–1.6 | 1.32 | 0.0017 | SWV | [52] |
| SSZ MIP-modified CPE | 0.01–1.0 | – | 0.0046 | DPV | [53] |
| Bismuth-film electrode | 5–31 | – | 1.4 | SWV | [54] |
| NiO/CNT CPE | 0.5–800 | 0.238 | 0.09 | SWV | [3] |
| Mercury electrode | 0.1–1.0 | – | 4.1 | AdSV | [1] |
| Pt/SWNT/GCE | 0.5–20 | – | 0.086 | SWV | [55] |
| MWCNTCOOH/BA-SPCE | 1.0–70 | – | 0.3 | DPV | [6] |
| $SmVO_4$@CNF/GCE | 0.009–445 | 4.03 | 0.0013 | AMP | [9] |
| $MnCo_2O_4/C_3N_4$ | 0.01–95.4 | 9.28 | 0.003 | DPV | [56] |
| ZnO–$Co_3O_4$ | 0.005–18.5 | 0.142 | 0.012 | PCA | [57] |
| $SmVO_4$@GOS/GCE | 0.02 – 667.74 | 6.231 | **0.00216** | **AMP** | **This work** |

*SWV* square wave voltammetry, *DPV* differential pulse voltammetry, *LSV* linear sweep voltammetry, *AdSV* adsorptive stripping voltammetry, *GCE* glassy carbon electrode, *CPE* carbon paste electrode, *SPCE* screen-printed carbon electrode, *MWCNTCOOH/BA* multiwalled carbon nanotubes/benzyl acetate, *PCA* photoelectrochemical analysis.

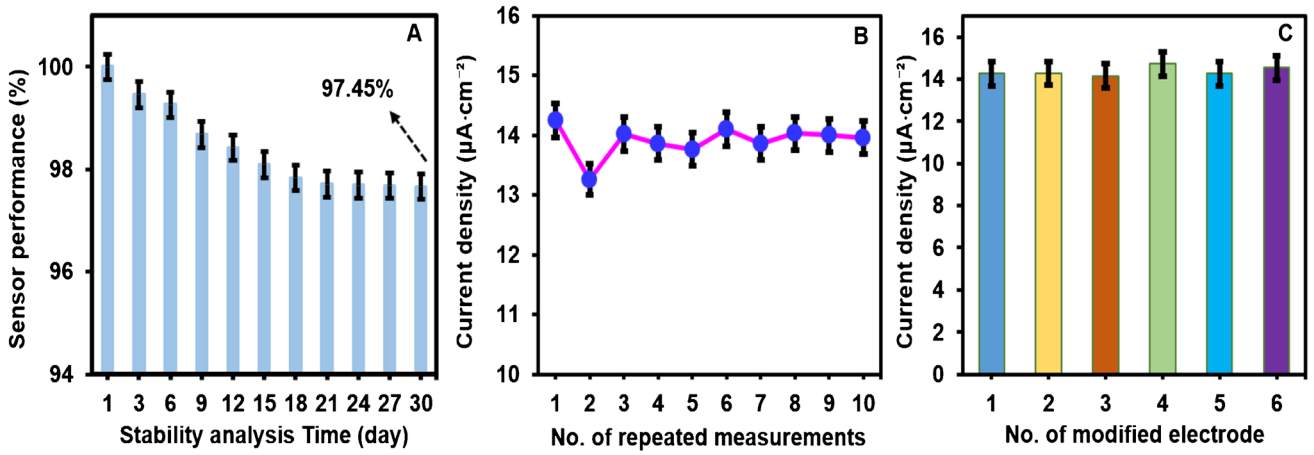


**Fig. 7** **A** Calibration plot for stability analysis up to 30 days. **B** Repeatability analysis of the $SmVO_4$@GOS modified electrode. **C** Reproducibility analysis of the modified sensor using six electrodes

(UA), dopamine (DA), paracetamol (PA), flutamide (Flu), nitrofurazone (NF), nitrofurantoin (NFT), hydrogen peroxide ($H_2O_2$), epinephrine (EPN), ciprofloxacin (CFX), norfloxacin (NFX), metronidazole (MTZ), chloramphenicol (CAP), paraoxon (PXN), fenitrothion (FTN), chlorpyrifos (CPF), dichlorvos (DCR), hydroquinone (HQ), catechol (CC), nitrate ions ($NO_3^-$), chlorine ions ($Cl^-$), and fenhexamid (FXD). Figure S3A shows no high changes in the oxidation peak current response, even with the addition of the abovementioned common interfering pharmaceuticals (drugs, herbicides, pesticides, fungicides, hydroquinone, catechol, flavonoids, pollutants, biogenic amines, ion species). Based on the literature and our experiments, dopamine, epinephrine, and uric acid are oxidized at 0.2, 0.31, and 0.38 V (Ag/AgCl) peak potentials, respectively. Mainly, those analytes are oxidized at below 0.6 V (Ag/AgCl). In this work, our modified $SmVO_4$@GOS/GCE electrode shows SSZ peak at above 0.8 V (Ag/AgCl). Therefore, those analytes have not affected our modified sensors toward SSZ detection. Moreover, interference aspect of ascorbic acid and sulfamethoxazole is checked in the presence of SSZ. There is no major difference in the SSZ peak response due to effective oxidation of SSZ.

Using 100 μM of SSZ, the amperometric response was recorded continuously for 30 days (once every 3 days). After every use of the electrode, it was placed at 4 °C (Fig. 7A). Even after 30 days, the $SmVO_4$@GOS/GCE electrode exhibited good stability and managed to retain 97.4% of its initial value. In addition, the repeatability of the bimetal oxide-based graphene oxide modified electrode was analyzed, and the RSD value of 3.26% is obtained (Fig. 7B). To better understand the precision of the electrode, the amperometric response toward the oxidation of 100 μM of SSZ was investigated by using six different electrodes ($SmVO_4$@GOS/GCE-1–6). The obtained RSD value of 3.26% indicates the excellent precision of the electrode (Fig. 7C).

**Table 2** Determination of SSZ in spiked biological samples at the $SmVO_4$@GOS modified electrode

| Real samples | Added (nM) | Found (nM) | | Recovery (%) | | RSD/ ± % ($n$ = 3) | |
|---|---|---|---|---|---|---|---|
| | | AMP | HPLC | AMP | HPLC | AMP | HPLC |
| Blood serum | 0 | 0 | 0 | 0 | 0 | 0 | 0 |
| | 50.0 | 48.9 | 49.0 | 97.8 | 98.0 | 2.13 | 1.89 |
| | 100 | 99.7 | 99.8 | 99.7 | 99.8 | 1.06 | 1.03 |
| | 200 | 197 | 198 | 98.5 | 99.0 | 2.14 | 1.49 |
| Urine sample | 0 | 0 | 0 | 0 | 0 | – | 0 |
| | 50.0 | 49.2 | 49.3 | 98.4 | 98.6 | 1.86 | 1.29 |
| | 100 | 98.7 | 99.1 | 98.7 | 99.1 | 1.98 | 1.34 |
| | 200 | 196 | 198 | 98 | 99.0 | 1.02 | 1.13 |

### *Practical applicability of $SmVO_4$@GOS/GCE toward SSZ*

Any fabricated electrode for the detection of pharmaceutical compounds needs to demonstrate its practical applicability using real-world samples, pharmaceutical formulations, etc. Human blood serum and urine samples were selected to study the oxidation of SSZ using $SmVO_4$@GOS/GCE. Details regarding the purchase of materials and the sample preparation method are given in the Supporting information. The recovery studies were performed by following a standard addition procedure. The original urine and blood serum failed to show any response toward the oxidation of SSZ. The amperometric response was monitored after spiking SSZ to the biological samples under optimum conditions, and the results are given in Table 2. The recovery ranges were 96.7–98.6% and 96.1–97.1% for the human serum and urine samples, respectively. These recovery results indicate that the fabricated electrode exhibited good amperometric response toward SSZ oxidation, even in the presence of unknown interferences. Thus, the fabricated $SmVO_4$@GOS/GCE proved to be an excellent amperometric probe for the effective oxidation of SSZ for day-to-day real-time applications.

## Conclusion

A deep eutectic solvent in association with the hydrothermal method was developed for the synthesis of samarium orthovanadate particles wrapped in graphene oxide sheets. The $SmVO_4$@GOS nanocomposite was used to modify a GCE for use as a working electrode for sensing an anti-rheumatic drug (SSZ). The amperometric technique was found to be more sensitive than CV, with a wide linear range of detection toward the detection of SSZ. The enhanced electrochemical behavior of $SmVO_4$@GOS/GCE was owing to the enhanced conductivity and increased surface area. The fabricated electrode demonstrated excellent selectivity in detecting SSZ in the presence of known drugs and unknown interferences. The most required parameter of an electrochemical sensor is its real-time application, which was perfectly met by $SmVO_4$@GOS/GCE. The additional advantage of the electrode is its stability and reproducibility. The electrochemical performance of $SmVO_4$@GOS/GCE toward the detection of SSZ indicated its high sensitivity, selectivity, stability, accuracy, and precision, and as a result, it is suitable for use in the medical and pharmaceutical industries.

**Supplementary Information** The online version contains supplementary material available at https://doi.org/10.1007/s00604-022-05498-w.

**Acknowledgements** This work was also funded by the Researchers Supporting Project Number (RSP-2021/266) King Saud University, Riyadh, Saudi Arabia.

**Funding** Financial support was from the Ministry of Science and Technology, MOST 110–2221-E-131–009, Taiwan, and Research Center for Intelligent Medical Devices of Ming Chi University of Technology, Taiwan. This work was also funded by the Researchers Supporting Project Number (RSP-2021/266) King Saud University, Riyadh, Saudi Arabia.

## Declarations

**Conflict of interest** The authors declare no competing interests.

## References

1. Kotouček M, Skopalová J, Michálková D (1997) Electroanalytical study of salazosulfapyridine and biseptol components at the mercury electrode. Anal Chim Acta 353:61–69
2. Jahani PM, Jafari M, Gupta VK, Agarwal S (2020) Electrochemical detection of sulfasalazine in real samples by and ionic liquid modified nanostructure 2@ SiO 4 O3 GO/Fe carbon paste electrode. Int J Electrochem Sci 15:6829–6840
3. Beitollahi H, Yoonesfar R (2017) Sensitive detection of sulfasalazine at a carbon paste electrode modified with NiO/CNT nanocomposite and ionic liquid in pharmaceutical and biological samples. Inorganic and Nano-Metal Chemistry 47:1441–1448
4. Koseoglu TS, Durgut A (2020) Development of a novel molecularly imprinted overoxidized polypyrrole electrode for the determination of sulfasalazine. Electroanalysis 32:2072–2081
5. Ahmadpour H, Hosseini SMM (2019) A solid-phase luminescence sensor based on molecularly imprinted polymer-CdSeS/ZnS quantum dots for selective extraction and detection of sulfasalazine in biological samples. Talanta 194:534–541
6. Sadeghi S, Garmroodi A (2014) Sensitive detection of sulfasalazine at screen printed carbon electrode modified with functionalized multiwalled carbon nanotubes. J Electroanal Chem 727:171–178
7. Wang J, Chang Y, Zhang P, Lie SQ, Gao PF, Huang CZ (2015) Cu2+-mediated fluorescence switching of gold nanoclusters for the selective detection of clioquinol. Analyst 140:8194–8200
8. Bondiolotti G, Pollera C, Pirola R, Bareggi S (2006) Determination of 5-chloro-7-iodo-8-quinolinol (clioquinol) in plasma and tissues of hamsters by high-performance liquid chromatography and electrochemical detection. J Chromatogr B 837:87–91
9. Baby JN, Sriram B, Wang S-F, George M (2021) Integration of samarium vanadate/carbon nanofiber through synergy: an electrochemical tool for sulfadiazine analysis. J Hazard Mater 408:124940
10. Nataraj N, Chen S-M (2021) Samarium vanadate nanospheres integrated carbon nanofiber composite as an efficient electrocatalyst for antituberculosis drug detection in real samples. Colloids Surf, A 617:126385
11. Mani V, Govindasamy M, Chen S-M, Karthik R, Huang S-T (2016) Determination of dopamine using a glassy carbon electrode modified with a graphene and carbon nanotube hybrid decorated with molybdenum disulfide flowers. Microchim Acta 183:2267–2275
12. Govindasamy M, Chen S-M, Mani V, Devasenathipathy R, Umamaheswari R, Santhanaraj KJ, Sathiyan A (2017) Molybdenum disulfide nanosheets coated multiwalled carbon nanotubes composite for highly sensitive determination of

chloramphenicol in food samples milk, honey and powdered milk. J Colloid Interface Sci 485:129–136
13. Nguyen T-D, Dinh C-T, Nguyen D-T, Do T-O (2009) A novel approach for monodisperse samarium orthovanadate nanocrystals: controlled synthesis and characterization. The J Physical Chemistry C 113:18584–18595
14. Babulal SM, Koventhan C, Chen SM, Hung W (2022) Construction of sphere like samarium vanadate nanoparticles anchored graphene nanosheets for enhanced electrochemical detection of nitrofurantoin in biological fluids. Compos B Eng 237:109847
15. Sakthivel M, Sukanya R, Chen S-M, Ho K-C (2018) Synthesis and characterization of samarium-substituted molybdenum diselenide and its graphene oxide nanohybrid for enhancing the selective sensing of chloramphenicol in a milk sample. ACS Appl Mater Interfaces 10:29712–29723
16. Xu X, Niu C, Duan M, Wang X, Huang L, Wang J, Pu L, Ren W, Shi C, Meng J (2017) Alkaline earth metal vanadates as sodium-ion battery anodes. Nat Commun 8:1–11
17. Andrukaitis E, Cooper JP, Smit JH (1995) Lithium intercalation in the divalent metal vanadates MeV2O6 (Me Cu Co, Ni, Mn or Zn). J Power Sources 54:465–469
18. Rajaji U, Govindasamy M, Sha R, Alshgari RA, Juang R-S, Liu T-Y (2022) Surface engineering of 3D spinel Zn3V2O8 wrapped on sulfur doped graphitic nitride composites: investigation on the dual role of electrocatalyst for simultaneous detection of antibiotic drugs in biological fluids. Compos B Eng 242:110017
19. Xiang L, Fan J, Zhong W, Mao L, You K, Yin D (2019) Heteroatom-induced band-reconstruction of metal vanadates for photocatalytic cyclohexane oxidation towards KA-oil selectivity. Appl Catal A 575:120–131
20. Selvan RK, Gedanken A, Anilkumar P, Manikandan G, Karunakaran C (2009) Synthesis and characterization of rare earth orthovanadate (RVO 4; R= La, Ce, Nd, Sm, Eu & Gd) nanorods/nanocrystals/nanospindles by a facile sonochemical method and their catalytic properties. J Cluster Sci 20:291–305
21. Ghotekar S, Pansambal S, Pagar K, Pardeshi O, Oza R (2018) Synthesis of CeVO4 nanoparticles using sol-gel auto combustion method and their antifungal activity. Nanochemistry Research 3:189–196
22. He Y, Wang Y, Zhao L, Wu X, Wu Y (2011) Preparation, characterization and activity evaluation of V2O5–LaVO4 composites under visible light irradiation. J Mol Catal A: Chem 337:61–67
23. Fan W, Song X, Bu Y, Sun S, Zhao X (2006) Selected-control hydrothermal synthesis and formation mechanism of monazite-and zircon-type LaVO4 nanocrystals. J Phys Chem B 110:23247–23254
24. Veldurthi NK, Eswar NK, Singh SA, Madras G (2018) Cocatalyst free Z-schematic enhanced H2 evolution over LaVO4/BiVO4 composite photocatalyst using Ag as an electron mediator. Appl Catal B 220:512–523
25. Liu X, Qin H, Fan W (2016) Enhanced visible-light photocatalytic activity of a gC 3 N 4/m-LaVO 4 heterojunction: band offset determination. Science Bulletin 61:645–655
26. Wang X, Zhang L, Lin H, Nong Q, Wu Y, Wu T, He Y (2014) Synthesis and characterization of a ZrO 2/gC 3 N 4 composite with enhanced visible-light photoactivity for rhodamine degradation. RSC Adv 4:40029–40035
27. E. Tamilalagan, M. Akilarasan, S.-M. Chen, T.-W. Chen, Y.C. Huang, Q. Hao, W. Lei. A sonochemical assisted synthesis of hollow sphere structured tin (IV) oxide on graphene oxide sheets for the low-level detection of environmental pollutant mercury in biological and foodstuff samples. Ultrasonics Sonochemistry, (2020) 105164.
28. Li T, Zhao L, He Y, Cai J, Luo M, Lin J (2013) Synthesis of g-C3N4/SmVO4 composite photocatalyst with improved visible light photocatalytic activities in RhB degradation. Appl Catal B 129:255–263
29. Muthumariappan A, Govindasamy M, Chen S-M, Sakthivel K, Mani V (2017) Screen-printed electrode modified with a composite prepared from graphene oxide nanosheets and Mn 3 O 4 microcubes for ultrasensitive determination of nitrite. Microchim Acta 184:3625–3634
30. Muthumariyappan A, Rajaji U, Chen S-M, Chen T-W, Li Y-L, Ramalingam RJ (2019) One-pot sonochemical synthesis of Bi2WO6 nanospheres with multilayer reduced graphene nanosheets modified electrode as rapid electrochemical sensing platform for high sensitive detection of oxidative stress biomarker in biological sample. Ultrason Sonochem 57:233–241
31. Li Q, Wu J-T, Liu Y, Qi X-M, Jin H-G, Yang C, Liu J, Li G-L, He Q-G (2021) Recent advances in black phosphorus-based electrochemical sensors: a review. Anal Chim Acta 1170:338480
32. Govindasamy M, Jian C-R, Kuo C-F, Hsieh A-H, Sie J-L, Huang C-H (2022) A chemiresistive biosensor for detection of cancer biomarker in biological fluids using CVD-grown bilayer graphene. Microchim Acta 189:1–12
33. Govindasamy M, Wang S-F, Huang C-H, Alshgari RA, Ouladsmane M (2022) Colloidal synthesis of perovskite-type lanthanum aluminate incorporated graphene oxide composites: electrochemical detection of nitrite in meat extract and drinking water. Microchim Acta 189:1–11
34. Nehru R, Hsu Y-F, Wang S-F, Dong C-D, Govindasamy M, Habila MA, AlMasoud N (2021) Graphene oxide@ Ce-doped TiO2 nanoparticles as electrocatalyst materials for voltammetric detection of hazardous methyl parathion. Microchim Acta 188:1–11
35. Li Q, Xia Y, Wan X, Yang S, Cai Z, Ye Y, Li G (2020) Morphology-dependent MnO2/nitrogen-doped graphene nanocomposites for simultaneous detection of trace dopamine and uric acid. Mater Sci Eng, C 109:110615
36. Li G, Zhong P, Ye Y, Wan X, Cai Z, Yang S, Xia Y, Li Q, Liu J, He Q (2019) A highly sensitive and stable dopamine sensor using shuttle-like α-Fe2O3 nanoparticles/electro-reduced graphene oxide composites. J Electrochem Soc 166:B1552
37. Liu H, Xiong R, Zhong P, Li G, Liu J, Wu J, Liu Y, He Q (2020) Nanohybrids of shuttle-like α-Fe2O3 nanoparticles and nitrogen-doped graphene for simultaneous voltammetric detection of dopamine and uric acid. New J Chem 44:20797–20805
38. Li F, Ni B, Zheng Y, Huang Y, Li G (2021) A simple and efficient voltammetric sensor for dopamine determination based on ZnO nanorods/electro-reduced graphene oxide composite. Surfaces and Interfaces 26:101375
39. Dağcı K, Alanyalıoğlu M (2016) Preparation of free-standing and flexible graphene/Ag nanoparticles/poly (pyronin Y) hybrid paper electrode for amperometric determination of nitrite. ACS Appl Mater Interfaces 8:2713–2722
40. Rajaji U, Manavalan S, Chen S-M, Govindasamy M, Chen T-W, Maiyalagan T (2019) Microwave-assisted synthesis of europium (III) oxide decorated reduced graphene oxide nanocomposite for detection of chloramphenicol in food samples. Compos B Eng 161:29–36
41. Errandonea D, Achary SN, Pellicer-Porres J, Tyagi AK (2013) Pressure-induced transformations in PrVO4 and SmVO4 and isolation of high-pressure metastable phases. Inorg Chem 52:5464–5469
42. Pei S, Zhao J, Du J, Ren W, Cheng H-M (2010) Direct reduction of graphene oxide films into highly conductive and flexible graphene films by hydrohalic acids. Carbon 48:4466–4474
43. Larachi FC, Pierre J, Adnot A, Bernis A (2002) Ce 3d XPS study of composite CexMn1− xO2− y wet oxidation catalysts. Applied Surface Science 195:236–250
44. Silversmit G, Depla D, Poelman H, Marin GB, De Gryse R (2004) Determination of the V2p XPS binding energies for different

vanadium oxidation states (V5+ to V0+). J Electron Spectrosc Relat Phenom 135:167–175
45. Saisree S, Aswathi R, Nair JA, Sandhya K (2020) Radical sensitivity and selectivity in the electrochemical sensing of cadmium ions in water by polyaniline-derived nitrogen-doped graphene quantum dots. New J Chem 45:110–122
46. Sasikumar R, Govindasamy M, Chen S-M, Chieh-Liu Y, Ranganathan P, Rwei S-P (2017) Electrochemical determination of morin in kiwi and strawberry fruit samples using vanadium pentoxide nano-flakes. J Colloid Interface Sci 504:626–632
47. Govindasamy M, Chen S-M, Mani V, Sathiyan A, Merlin JP, Al-Hemaid FM, Ali MA (2016) Simultaneous determination of dopamine and uric acid in the presence of high ascorbic acid concentration using cetyltrimethylammonium bromide–polyaniline/activated charcoal composite. RSC Adv 6:100605–100613
48. Lahcen AA, Rauf S, Aljedaibi A, de Oliveira Filho JI, Beduk T, Mani V, Alshareef HN, KN, (2021) Salama Laser-scribed graphene sensor based on gold nanostructures and molecularly imprinted polymers: application for Her-2 cancer biomarker detection. Sensors and Actuators B: Chemical 347:130556
49. Nigović B, Hocevar SB (2011) Antimony film electrode for direct cathodic measurement of sulfasalazine. Electrochim Acta 58:523–527
50. Buoro RM, Diculescu VC, Lopes IC, Serrano SH, Oliveira-Brett AM (2014) Electrochemical oxidation of sulfasalazine at a glassy carbon electrode. Electroanalysis 26:924–930
51. Msagati TA, Ngila JC (2002) Voltammetric detection of sulfonamides at a poly (3-methylthiophene) electrode. Talanta 58:605–610
52. Amani-Beni Z, Nezamzadeh-Ejhieh A (2018) NiO nanoparticles modified carbon paste electrode as a novel sulfasalazine sensor. Anal Chim Acta 1031:47–59
53. Sadeghi S, Motaharian A, Moghaddam AZ (2012) Electroanalytical determination of sulfasalazine in pharmaceutical and biological samples using molecularly imprinted polymer modified carbon paste electrode. Sens Actuators, B Chem 168:336–344
54. Nigović B, Šimunić B, Hocevar S (2009) Voltammetric measurements of aminosalicylate drugs using bismuth film electrode. Electrochim Acta 54:5678–5683
55. Savalia R, Chatterjee S (2018) Sensing of sulfasalazine—cysteine transporter inhibitor with platinum nanoflowers decorated on carbon nanotubes by electrochemical reduction. Sens Actuators, B Chem 277:39–46
56. Sriram B, Baby JN, Hsu YF, Wang SF, Benadict Joseph X, George M, Veerakumar P, Lin KC (2021) MnCo2O4 microflowers anchored on P-doped g-C3N4 nanosheets as an electrocatalyst for voltammetric determination of the antibiotic drug sulfadiazine. ACS Appl Electronic Mater 3:3915–3926
57. Velmurugan S, Yang TC-K, Chen S-W, Chen J-N (2021) Metal-organic frameworks derived ZnO-Co3O4 pn heterojunction photocatalyst for the photoelectrochemical detection of sulfadiazine. J Environ Chem Eng 9:106169